Graphene derivatives-based PVA hydrogel electrolyte for supercapacitors

A. Méndez-Reséndiz, S.A. Pérez-García, L. Licea-Jiménez

Hydrogel electrolytes were synthesized using polyvinyl alcohol (PVA) and various graphene derivatives, including graphene oxide (GO), exfoliated graphene (GEX), reduced graphene oxide (rGO), and selectively oxidized graphene (SOG). The effects of these graphene derivatives on the gel structure were analyzed using Fourier-transform infrared spectroscopy (FTIR), X-ray diffraction (XRD), thermogravimetric analysis (TGA), and rheological measurements. Additionally, the influence of the water-to-ethylene glycol ratio on the gel properties was assessed. Incorporating graphene derivatives enhanced hydrogen bonding within the hydrogel network, depending on the oxygen functional groups and defect density of the graphene materials, leading to improved structural stability. While ethylene glycol contributes to the gel formation, adding graphene derivatives further enhances the hydrogel's mechanical properties, maintaining a high storage modulus and preserving ionic conductivity. These findings provide valuable insights for developing supercapacitors with an optimal balance between mechanical strength and energy storage efficiency.

Introduction

Supercapacitors are highly effective energy storage devices that meet the needs of various applications such as wearable technology, flexible electronics, electric vehicles, and aerospace systems due to their high-power density, rapid charge-discharge rates, lightweight, and flexibility [1-3]. However, the overall performance of these devices is primarily limited by the structure and properties of their key components, including electrodes and electrolytes. In response to this challenge, extensive research has been focused on exploring nanostructured materials, mainly two-dimensional (2D) materials like graphene and its derivatives, for potential improvements [4,5]. Successful integration of these materials as reinforcements requires that electrolytes possess key characteristics such as high load-bearing capacity, mechanical strength, and thermal and rheological stability. Hydrogels are promising candidates for achieving requirements, offering high ionic conductivity, flexibility, and relatively strong mechanical properties [6]. Polyvinyl alcohol (PVA), one of the most widely used water-soluble polymers, has been shown to provide the required properties for hydrogel electrolytes [3,7]. However, PVA alone has drawbacks such as freezing at low temperatures (under 0 °C), lower ionic conductivity compared to liquid electrolytes, and mechanical properties that are compromised under stress limiting its operational range for various applications [8-10]. Organic solvents like ethylene glycol have been introduced to lower the freezing point and extend the device's temperature range [11] to mitigate this issue. Unfortunately, adding anti-freezing components decreases ionic conductivity, negatively impacting device performance. Recent studies have demonstrated that graphene derivatives can significantly improve ionic conductivity while enhancing the hydrogel's mechanical properties [3,6,12,13] due to their exceptional electronic and mechanical characteristics. For hydrogels, mechanical properties can be extracted through rheological characterization like viscosity measurements and the obtention of storage (G') and loss modulus (G"), which are related to the elastic and viscous behavior, respectively. Giving information about the mechanical stability of the hydrogels [9,12].

In this work, hydrogel electrolytes were prepared using various graphene derivatives, including graphene oxide (GO), exfoliated graphene (GEX), reduced graphene oxide (rGO), and selectively oxidized graphene (SOG). The effects of these different graphene derivatives, along with the influence of the water-to-ethylene glycol ratio, were examined using Fourier-transform infrared spectroscopy (ATR-FTIR), X-ray diffraction (XRD), thermogravimetric analysis (TGA), ionic conductivity measurements, and rheological properties (viscosity, loss modulus, and storage modulus).

Material and methods

Graphite nanoparticles (GNPs) were used as starting material supplied by ACS materials with a thickness of 40 nm and lateral size of 400-600 nm. $KMnO_4$, KNO_3, HCl, and H_2SO_4 were purchased from CTR Scientific. Ethanol, H_2O_2, and methanol were purchased from J.T. Baker. All the chemicals were used as received.

GO was synthesized using a modified Hummers' method, as reported elsewhere [14,15]. 0.25 g of GNPs were oxidized in 15 ml of H_2SO_4 and 0.15 g of KNO_3 with 1.5 g of $KMnO_4$. The reaction lasted six hours in an ice bath (T < 14 °C). The reaction was quenched with 50 ml of DI H_2O and 1.5 ml of 30% H_2O_2. Then, the resulting dispersion was centrifuged at 3500 rpm for 10 min, removing the supernatant. Afterward, 100 ml of HCl 10% was added to the residue and centrifuged under the same conditions. Then, the sample was washed 3 times with DI H_2O. Afterward, 40 ml of DI H_2O was added, followed by exfoliation in an ultrasonic bath for one hour, then centrifuged at 3500 rpm for an additional hour, recovering the supernatant (GO dispersion) to be used as the material.

Abraham Méndez-Reséndiz, Sergio Alfonso Pérez-García ✉, Liliana Licea-Jiménez ✉
[a]*Centro de Investigación en Materiales Avanzados S.C. (CIMAV), Subsede Monterrey. Apodaca, N.L., 66628, México.*
[b]*Group of Polymer Nanocomposites, (CIMAV), Unidad Monterrey Apodaca, N.L., 66628, México.*

Received: April 28th, 2025.
Accepted: September 9th, 2025.
Published: October 28th, 2025.
© 2025 by the authors. Creative Commons Attribution
https://doi.org/10.47566/2025_syv38_1-251001

From GO, 120 mg ml^{-1} of ascorbic acid (NH_4OH pH 10) was added to the dispersion. The reaction was carried out with stirring for 24 hours. 10 % HCl was added to precipitate reduced graphene oxide (rGO), and the supernatant was centrifuged to remove it. Then, the samples were dispersed in DI water and vacuum filtrated to obtain rGO powder.

Selectively oxidized graphene (SOG) was synthesized following the same modified Hummers' method but under mild conditions, reducing the oxidant ratio tenfold and the reaction time to 30 min [16]. Afterward, the sample was centrifuged at 4500 rpm for 10 min, discarding the supernatant and washing the precipitate with 10% HCl. This was followed by three centrifuge washing steps with DI water. For one hour, the precipitate obtained was exfoliated in DI water using an ultrasonic bath to obtain SOG dispersion.

Using the same starting material, exfoliated graphene (GEX) was obtained. A 5 mg ml^{-1} GNP dispersion was prepared in a 50% v/v mixture of water and ethanol. Afterward, this solution was exfoliated with an ultrasonic probe for 2 hours, obtaining a GEX dispersion.

Sample preparation

First, to obtain the hydrogels, PVA (Sigma-Aldrich, M_w 89,000-98,000, 99% hydrolyzed) was used as a polymer matrix at 10% wt, with ethylene glycol (EG) at 0.5% v/v and H_3PO_4 at 0.5% v/v. This is the formulation without reinforcement. Then, formulations using GO, GEX, and rGO at 0.5% wt. as reinforcements were prepared, dispersing the graphene derivatives using an ultrasonic probe before polymer addition, maintaining the same concentration of EG and H_3PO_4 for all samples. These samples were labeled PVA, GO/PVA, GEX/PVA, and rGO/PVA.

To evaluate the influence of EG on the hydrogel formulation, the same procedure mentioned earlier was followed using GO, GEX, and SOG at 0.5% wt. and H_3PO_4 at 0.5% v/v while varying EG content. The water-to-ethylene glycol (H_2O: EG) ratios used were 2:1, 3:1, and 4:1. These samples were labeled as previously indicated, adding the water-to-ethylene glycol ratio for each sample noted in parentheses.

Materials and samples characterization

First, the morphology of the hydrogels was examined using scanning electron microscopy (SEM) with a FEI Nova NanoSem200 instrument. The hydrogels were sliced and mounted transversely to observe the internal structure of the samples.

ATR-FTIR was performed using a Nicolet is50 spectrometer ranging from 4000 to 400 cm^{-1} to observe the functional groups in the samples and the interaction between the matrix and the fillers.

Thermogravimetric analysis of the different samples was performed using SDT Q600, TA Instruments in a nitrogen atmosphere to observe the loss/desorption of the various functional groups.

The X-ray diffraction (XRD) of the hydrogels was analyzed using deposited films with an Analytical Empyrean diffractometer employing Cu Kα radiation (1.540598 Å) in grazing incidence mode.

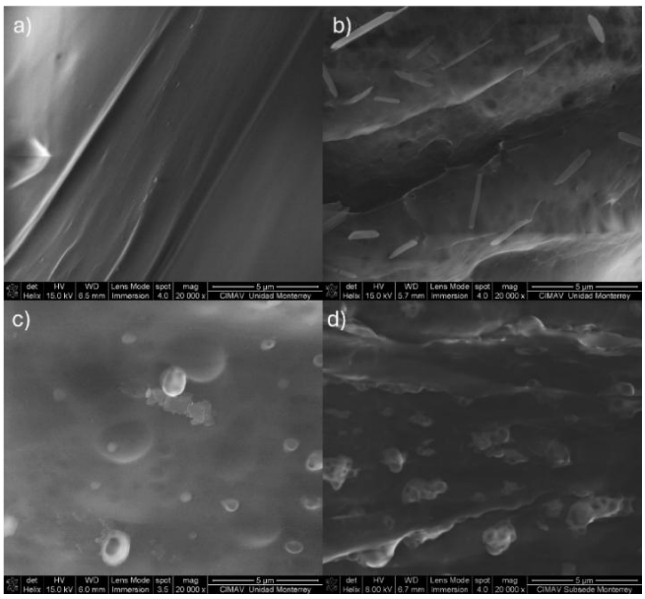

Figure 1. SEM micrographs of a) PVA gel, b) GO/PVA gel, c) GEX/PVA gel, and d) rGO/PVA gel.

The ionic conductivity of the different samples was measured using the Oakton pH/Conductivity/TDS/°C meter of the fresh samples obtained after the PVA aggregation.

The rheological characterization of the samples was conducted using a rotational rheometer, AR G2 from TA Instruments. This process determined the viscosity of the various samples, as well as the storage modulus (G') and the loss modulus (G''), which are related to the mechanical properties of the hydrogels.

Results and discussion

Figure 1 displays SEM micrographs of the various hydrogels obtained. In the micrograph of the PVA hydrogel without graphene derivatives (Figure 1a), a homogeneous structure with minimal porosity is observed, attributed to the ordering of the polymer chains [7]. The porosity significantly increases in all samples reinforced with graphene derivatives (Figures 1b-d) due to the formation of channels during polymer bonding, facilitated by the interaction of graphene derivatives with the polymer matrix. Specifically, the GO-reinforced hydrogel exhibits larger pores, likely due to the abundance of oxygen functional groups in the GO structure [15], which can interact with hydroxyl groups in the PVA chains, thereby enhancing cross-linking. Overall, the increased porosity is beneficial, as it provides diffusion pathways for ions, thereby improving ionic conductivity and enhancing the capacitance of supercapacitors. However, pore size plays a decisive role in device performance, which varies depending on the specific graphene derivative [17,18]. Figures 1c-d show the SEM micrographs for GEX/PVA and rGO/PVA, respectively, where the incorporation of GEX and rGO induces the formation of blister-like structures.

Figure 2a displays the FTIR spectra of the different PVA hydrogels, where distinct peaks are observed at 3250, 2943,

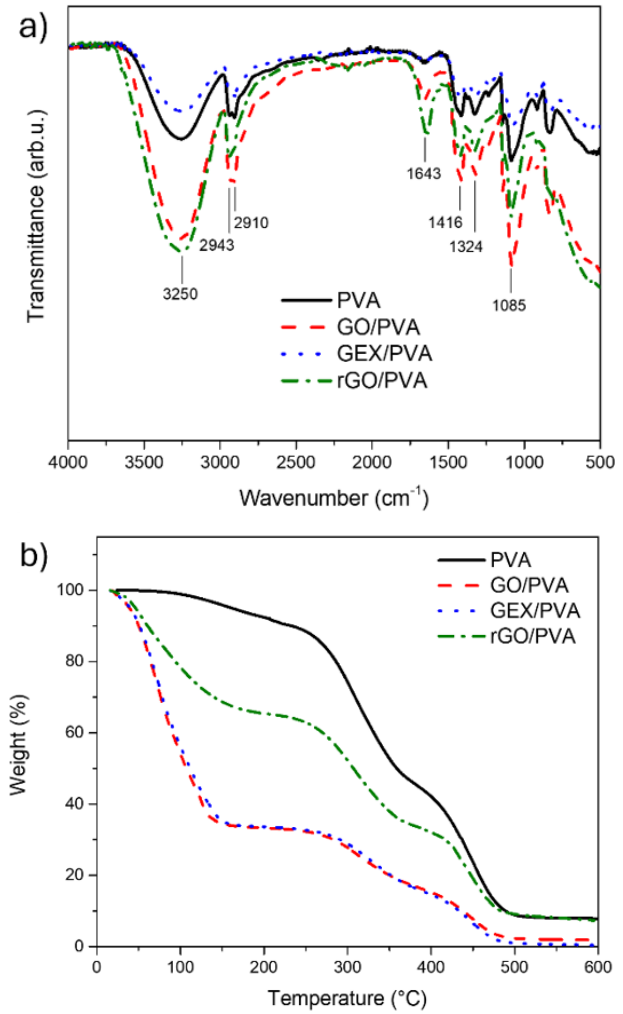

Figure 2. a) FTIR spectra and b) TGA graphs of the different hydrogels obtained.

2910, 1643, 1416, 1324, and 1085 cm^{-1}. These peaks correspond to O-H stretching, asymmetric CH_2 stretching, symmetric CH_2 stretching, C=O carbonyl stretching, CH_2 bending, CH wagging, and CO stretching, respectively [19-21]. Notably, the peak at 3250 cm^{-1}, linked to O-H stretching, demonstrates a significant change in shape, particularly in the GO/PVA and rGO/PVA samples. This change suggests enhanced hydrogen bonding between the oxygen-rich graphene derivatives and the hydroxyl groups of PVA. In Figure 2b, the TGA results reveal that samples containing graphene derivatives exhibit more significant mass loss than bare PVA at approximately 100 °C, indicating higher water retention. This behavior is likely due to the increased interaction between water molecules and the graphene derivatives within the hydrogel matrix. Water retention in gel electrolytes is a key factor for sustaining continuous ionic pathways, as water serves as the medium for ion transport and is therefore critical for maintaining high ionic conductivity. In general, higher water retention enhances ionic conductivity and can extend the electrochemical stability window of supercapacitors. However, excessive water retention may cause swelling and

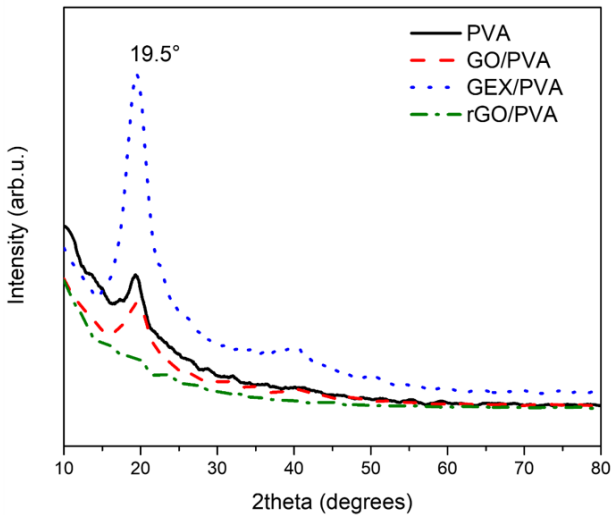

Figure 3. XRD diffractograms of the different hydrogels with graphene derivatives.

mechanical instability, while insufficient retention limits ionic transport and reduces conductivity. Thus, the design of gel electrolytes requires a careful balance between these opposing effects [22,23]. The incorporation of graphene derivatives with different oxidation states and surface functionalities provides a strategy to tune this balance and optimize electrochemical performance under diverse operating conditions.

Figure 3 presents the XRD diffractograms for the different hydrogels, showing a prominent peak at 19.5°, corresponding to the crystalline domain of the PVA chains [21]. The peak of the GO hydrogel remains nearly identical to that of the bare PVA, indicating that the relative order of the polymer chains is preserved. In contrast, the GEX/PVA sample increases peak intensity, suggesting an enhancement in the polymer crystallinity. This effect is likely due to the interaction between the polymer chains and the highly crystalline GEX, which acts as a template. Conversely, in the hydrogel rGO/PVA, the peak at 19.5° is almost absent,

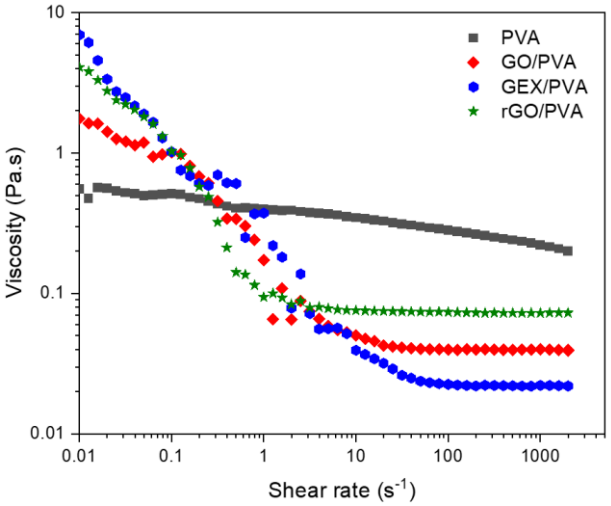

Figure 4. Viscosity vs shear rate for the different hydrogels with graphene derivatives.

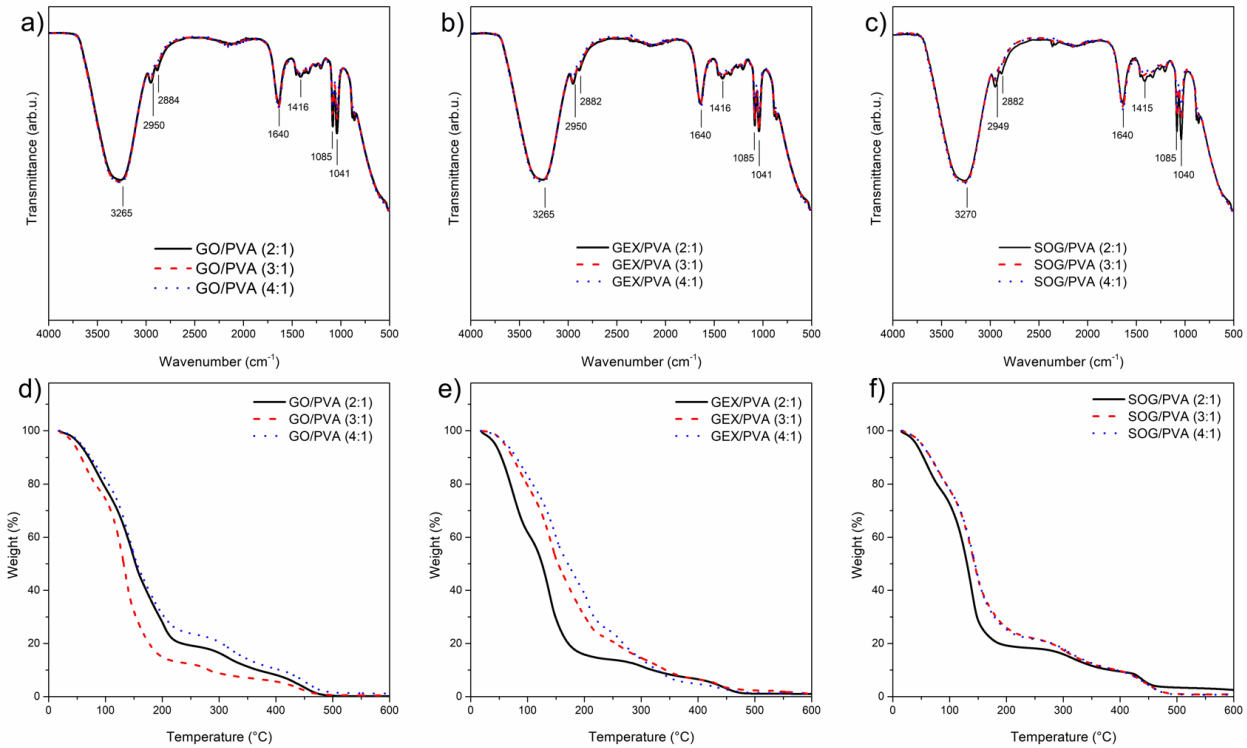

Figure 5. Results of the PVA hydrogels with varying H_2O:EG ratios for the different reinforcements, FTIR spectra for: a) GO/PVA, b) GEX/PVA, c) SOG/PVA, and TGA thermograms for samples: d) GO/PVA, e) GEX/PVA, f) SOG/PVA.

indicating a significant disruption in the polymer chain ordering. This loss of order is likely caused by numerous defects in rGO, which commonly exhibit wrinkling, thus interfering with the crystallinity of the PVA. In general, the degree of crystallinity in hydrogels is closely related to ionic conductivity: amorphous regions facilitate ion transport by providing more flexible diffusion pathways, while specific crystalline ordering can also promote ionic mobility under certain conditions [24,25].

Figure 4 presents the viscosity as a function of shear rate, where adding graphene derivatives leads to an increase in viscosity at low shear rates compared to bare PVA. This suggests that graphene derivatives interact with the polymer chains, altering the Newtonian behavior of the hydrogel and inducing a shear-thinning response [26,27]. These interactions between the PVA chains and the graphene fillers at higher shear rates diminish, reducing viscosity. This viscosity, analogous to the other parameters, influences ionic conductivity, as increased viscosity limits ion mobility.

The water-to-ethylene glycol ratio was modified after observing the effect of adding the different graphene derivatives. For this analysis, rGO was replaced with SOG since they exhibit similar oxygen concentrations, and SOG presents better processability in aqueous solvents. To evaluate the effect of ethylene glycol (EG) concentration on gel formation and the presence of graphene derivatives, Figure 5a-c shows that the FTIR spectra display the same peaks as previously observed. The peak corresponding to O-H stretching (~3265 cm^{-1}) is blue-shifted compared to bare PVA (3250 cm^{-1}), indicating interactions between PVA, EG, and graphene derivatives, with SOG exhibiting the most significant shift. In the TGA analysis (Figure 5d-f), the increased EG concentration correlates with a steeper mass loss after 100 °C, reflecting the solvent's influence on the thermal stability of the hydrogels, showing consistent trends across the different graphene derivatives.

Rheological experiments were conducted to analyze the impact of varying concentrations of ethylene glycol (EG) and different graphene derivatives on the gel structure. Figure 6 illustrates the viscosity as a function of shear rate for the different hydrogels. All hydrogels exhibit shear-thinning behavior, consistent with the addition of graphene derivatives. A significant increase in viscosity is observed with higher EG content, suggesting that the solvent strongly promotes gel formation, likely due to enhanced hydrogen bonding. It is also evident that the type of graphene derivative influences viscosity. SOG samples showed the highest viscosity (Figure 6c), likely because this material retains mechanical stiffness similar to GEX (Figure 6b) and contains oxygen functional groups that can anchor the PVA chains. In contrast, the lower viscosity observed in the GEX samples may be attributed to the absence of these oxygen functional groups, which reduces cross-linking and results in lower interaction with the polymer chains. Meanwhile, the GO samples (Figure 6a) showed a higher viscosity than GEX, likely resulting from the greater density of oxygen groups that promote stronger interfacial interactions with PVA. Ionic conductivity measurements for these samples are presented in Figure 7. A wide variation in conductivity is observed, which can be correlated with the different structural and physicochemical properties discussed earlier, such as porosity, crystallinity, water retention, and viscosity. It is worth noting that a H_2O:EG ratio of 2:1 consistently produced the most stable free-standing gels, whereas other

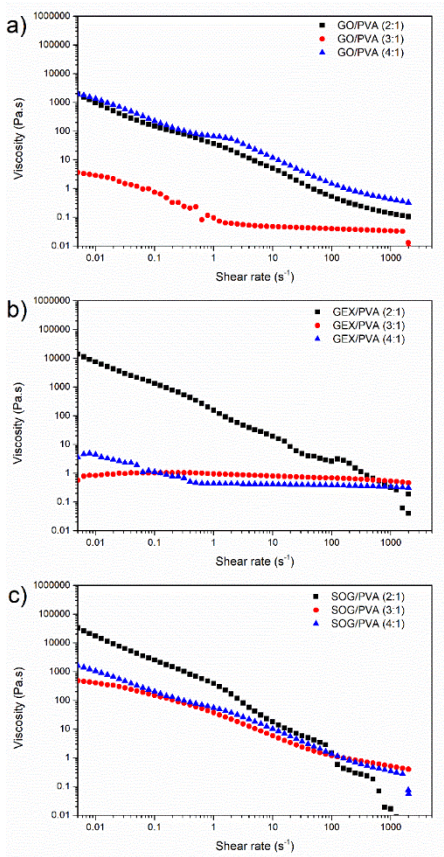

Figure 6. Viscosity vs shear rate graph for the PVA hydrogels with the different graphene derivatives; a) GO/PVA, b) GEX/PVA, and c) SOG/PVA.

ratios retained a partially liquid-like character. Based on these results, the 2:1 ratio was selected for further analysis of storage (G') and loss (G'') modulus determination, as these samples exhibited better gel formation. Table 1 presents the ionic conductivity measurements for the different hydrogels, which can be correlated with the viscosity values obtained. Higher viscosity generally corresponds to lower ionic conductivity, as expected due to the reduced ion mobility. However, it was observed that for GEX/PVA, the ionic conductivity increased with respect to GO/PVA sample even when the viscosity increased by ~ 450%. For SOG/PVA, the ionic conductivity only decreased by ~ 25% with respect to the GO sample, but the viscosity increased by ~ 1,140%.

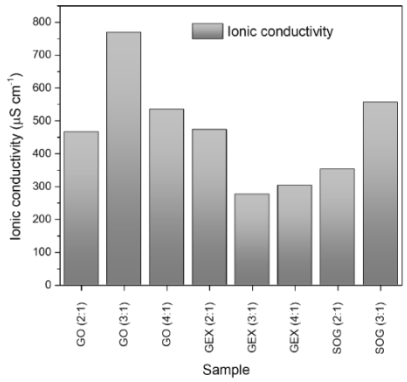

Figure 7. Ionic conductivity of the different samples with the graphene derivatives and different concentrations of EG.

Table 1. Ionic conductivity of the different PVA hydrogels.

Sample	Ionic conductivity (μS cm^{-1})	Viscosity (Pa·s)
GO/PVA (2:1)	466	3,040
GEX/PVA (2:1)	473	13,923
SOG/PVA (2:1)	353	34,665

This behavior can be attributed to the exceptional conductivity properties of GEX and SOG materials, which preserve ionic transport despite higher viscosity [16]. These results suggest that the incorporation of graphene derivatives enhances the overall properties of the gels, resulting in a more substantial structure while preserving ionic conductivity.

Figure 8 illustrates the storage (G') and loss (G'') modulus as a function of oscillatory stress for the different hydrogels. G' represents the energy stored in the elastic structure of the hydrogel; when G' exceeds G'', the hydrogel can be considered predominantly elastic [28]. In contrast, G'' corresponds to the viscous component, representing the amount of energy dissipated; if G'' surpasses G', it indicates a loss of the hydrogel's structural integrity. The three samples with the different graphene derivatives show $G' > G''$, indicating successful hydrogel formation. However, the type of graphene derivative significantly influences the

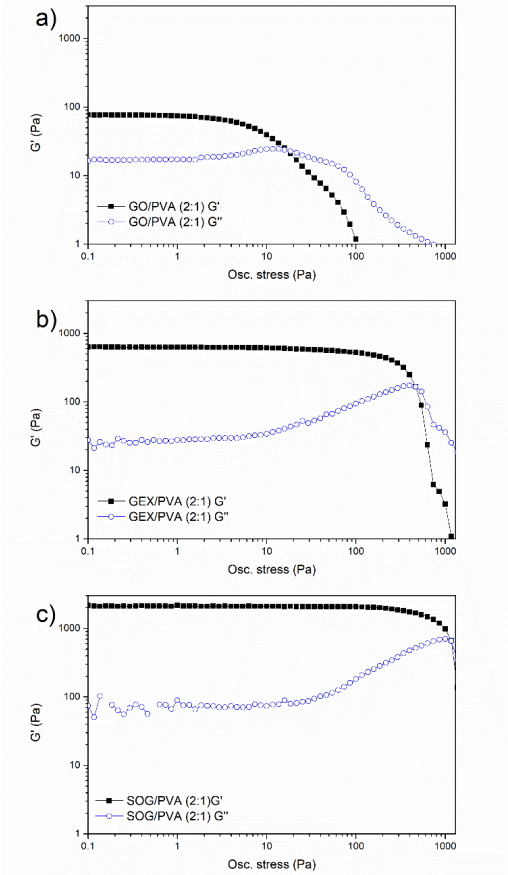

Figure 8. Storage (G') and loss (G'') modulus were obtained for the different hydrogels a) GO/PVA, b) GEX/PVA, and c) SOG/PVA.

hydrogel structure. GO hydrogel exhibited lower values for both G' and G'' (Figure 8a), losing the gel integrity at relatively low oscillatory stress. Besides, GEX and SOG displayed higher modulus values than GO (Figure 8b-c). This suggests that GEX and SOG enhance the mechanical properties of the hydrogel, likely due to their inherent mechanical stiffness. SOG, in particular, maintained the highest G' values even at higher stress levels, indicating a more stable structure. These results confirm that the mechanical properties of the hydrogels can be tailored by selecting specific graphene derivatives with the desired characteristics.

Conclusions

This study demonstrates that polyvinyl alcohol (PVA)-based hydrogel electrolytes reinforced with graphene derivatives exhibit improved mechanical and ionic transport properties, positioning them as promising candidates for energy storage applications such as supercapacitors. The incorporation of graphene oxide (GO), exfoliated graphene (GEX), reduced graphene oxide (rGO), and selectively oxidized graphene (SOG) alters the gel structure through hydrogen bonding and polymer–filler interactions, resulting in distinct effects on porosity, water retention, crystallinity, and viscoelastic behavior.

Overall, the results highlight that the impact of graphene derivatives is highly dependent on their structure and surface chemistry. GO enhances porosity and water retention but provides modest mechanical reinforcement. GEX contributes to mechanical stiffness but shows limited chemical interaction with PVA chains. rGO disrupts the polymer ordering due to its structural defects, compromising stability. In contrast, SOG emerges as the optimal filler, offering a unique combination of high mechanical modulus, structural stability, and preserved ionic conductivity. This balance between robust gel structure and efficient ion transport underscores the importance of tailoring the filler chemistry to optimize hydrogel electrolytes.

These findings provide new insights into the rational design of reinforced polymer electrolytes and contribute to the development of next-generation flexible supercapacitors with enhanced durability and energy storage capacity.

Acknowledgements

The authors acknowledge the US Army Research Office (ARO) supported this work under Grant W911NF-23-1-0301.

We would also like to thank the technical staff of CIMAV Campus Monterrey: Nayely Pineda Aguilar for SEM micrographs, Patricia Cerda Hurtado for the rheological and thermal characterizations, and Lilia Magdalena Bautista Carrillo for the FTIR analysis.

References

[1]. H. Zhou, H. Li, L. Li, T. Liu, G. Chen, Y. Zhu, L. Zhou, H. Huang, *Mater. Today Energy* **24**, 100924 (2022).
[2]. E.S. Greenhalgh, S. Nguyen, M. Valkova, N. Shirshova, M.S. Shaffer, A. Kucernak, *Compos. Sci. Technol.* **235**, 109968 (2023).
[3]. H. Zheng, R. Guan, Q. Liu, K. Ou, D.-s. Li, J. Fang, Q. Fu, Y. Sun, *Electrochim. Acta* 424, 140644 (2022).
[4]. G. Qi, S. Nguyen, D.B. Anthony, A.R.J. Kucernak, M.S.P. Shaffer, E.S. Greenhalgh, *Multifunct. Mater.* **4**, 034001 (2021).
[5]. R. Lakra, R. Kumar, P.K. Sahoo, D. Thatoi, A. Soam, *Inorg. Chem. Commun.* **133**, 108929 (2021).
[6]. H. Lu, S. Zhang, L. Guo, W. Li, *RSC Adv.* **7**, 51008 (2017).
[7]. H. Yu, N. Rouelle, A. Qiu, J.-A. Oh, D.M. Kempaiah, J.D. Whittle, M. Aakyiir, W. Xing, J. Ma, *ACS Appl. Mater. Interfaces* **12**, 37977 (2020).
[8]. C. Tang, Y. Yao, M. Li, Y. Wang, Y. Zhang, J. Zhu, L. Wang, L. Li, *Adv. Funct. Mater.* **35**, 2417207 (2025).
[9]. S. Alipoori, S. Mazinani, S.H. Aboutalebi, F. Sharif, *J. Energy Storage* **27**, 101072 (2020).
[10]. Z. Liu, J. Zhang, J. Liu, Y. Long, L. Fang, Q. Wang, T. Liu, *J. Mater. Chem. A* **8**, 6219 (2020).
[11]. Q. Rong, W. Lei, J. Huang, M. Liu, *Adv. Energy Mater.* **8**, 1801967 (2018).
[12]. Y. Huang, M. Zhang, W. Ruan, *J. Mater. Chem. A* **2**, 10508 (2014).
[13]. N. Devi, R. Kumar, S. Singh, R.K. Singh, *Crit. Rev. Solid State Mater. Sci.* **49**, 72 (2022).
[14]. U.A. Méndez-Romero, S.A. Pérez-García, Q. Fan, E. Wang, L. Licea-Jiménez, *RSC Adv.* **10**, 29432 (2020).
[15]. M. Velasco-Soto, S. Pérez-García, J. Alvarez-Quintana, Y. Cao, L. Nyborg, L. Licea-Jiménez, *Carbon* **93**, 967 (2015).
[16]. A. Méndez-Reséndiz, U.A. Méndez-Romero, R.A. Mendoza-Jiménez, B.A. Abdulahi, S.A. Pérez-García, E. Wang, L. Licea-Jiménez, *FlatChem* **38**, 100483 (2023).
[17]. R. Eslami, A. Malekkhouyan, P. Santhirakumaran, M. Mehrvar, H. Zarrin, *Small* **21**, 2410817 (2025).
[18]. G. Ruano, J.I. Iribarren, M.M. Pérez-Madrigal, J. Torras, C. Alemán, *Polymers* **13**, 1337 (2021).
[19]. A. Kharazmi, N. Faraji, R.M. Hussin, E. Saion, W.M.M. Yunus, K. Behzad, *Beilstein J. Nanotechnol.* **6**, 529 (2015).
[20]. I.M. Jipa, A. Stoica, M. Stroescu, L.-M. Dobre, T. Dobre, S. Jinga, C. Tardei, *Chem. Pap.* **66**, 138 (2012).
[21]. H. Abral, A. Atmajaya, M. Mahardika, F. Hafizulhaq, D. Handayani, S. Sapuan, R. Ilyas, *J. Mater. Res. Technol.* **9**, 2477 (2020).
[22]. Y. Qian, Y. Yu, W. Wu, Q. Fan, C. Chai, J. Hao, *Chem.-Eur. J.* **29**, e202300123 (2023).
[23]. X. Ye, H. Huang, L. Chen, Y. Wang, M. Weng, L. Zhang, Z. Luo, *Chem. Eng. J.* **483**, 149158 (2024).
[24]. A. Gupta, A. Jain, S. Tripathi, *J. Polym. Res.* **28**, 235 (2021).
[25]. S.S. Soni, K.B. Fadadu, A. Gibaud, *Langmuir* **28**, 751 (2012).
[26]. T. Javanbakht, E. David, *J. Thermoplast. Compos. Mater.* **35**, 651 (2022).
[27]. T. Javanbakht, *UJMEMS* **7**, 23 (2021).
[28]. A. Vinod, R. Tadmor, D. Katoshevski, E. Gutmark, *Gels* **9**, 555 (2023).

© 2025 by the authors; licensee SMCTSM, Mexico. This article is an open access article distributed under the terms and conditions of the Creative Commons Attribution license (http://creativecommons.org/licenses/by/4.0/).